

# Method and setup to increase power density threshold for image distinguishing by CCD camera

A. CHIRITA\*

Semiconductors Physics and Devices Laboratory, Research and Innovation Institute, Moldova State University, Chisinau, Republic of Moldova

Image recording of photosensitive objects, such as biological objects, whose biological and chemical activity can change as a function of light level, can be obtained at power densities from the object less than the minimal power density that can be registered by digital camera used. The rasterized images, at power densities from the object practically nine times less than the power density threshold for the digital camera used, were recorded and distinguished.

(Received February 18, 2020; accepted October 21, 2020)

**Keywords:** Laser beams interference, CCD Camera, Image processing

## 1. Introduction

In work [1], the review of various “interaction-free” visualization systems is presented, which make it possible to obtain optical images of photosensitive objects with less than the usual expected amount of light absorbed or scattered by the object. The proposed methods allow the study of biological systems, such as cells whose biological and chemical activity can change as a function of light level [1]. In work [2] an enhancement method of low-light-level images captured via a color-plus-mono camera is presented. The camera consists of two horizontally separate image sensors, which simultaneously captures both color and mono image pairs of the same scene. The proposed algorithm of image fusion between the color and mono image pair allows improving the image quality during low light shooting. In work [3] a method, that exploits the principle of diffuse scattering to apply and remove the shaped function signal for low-light-level image detection was proposed. To solve the problem of low-light-level image detection, a LED is used to illuminate the image sensor directly by the principle of diffuse scattering, rather than the object. The experiment results verify that the proposed method can maintain the capability of upgrading the sensitivity of the image sensor and improve the imaging speed in low-light-level detection. The possibility of photo-thermoplastic carriers sensitivity increase by an additional light-up of a carrier, rather than the object, during the recording process, was presented in work [4]. It was shown that additional illumination of photo-thermoplastic carriers by laser radiation with the wavelength, which is different from the hologram recording wavelength, increases the holographic sensitivity threshold of photo-thermoplastic carriers.

The purpose of this work is to increase the distinguishability of the image recorded by the digital camera at a low power density from the object.

## 2. Experimental setup

The principal scheme of the experimental setup is presented in Fig. 1. The plane-parallel coherent laser beam (1, Fig. 1), with the wavelength of  $\lambda = 532 \text{ nm}$  ( $P = 50 \text{ mW}$ , coherence length  $> 50 \text{ m}$ ), passes through the cube-divider (2) and is divided into two beams  $I_1$  and  $I_2$ . The beams  $I_1$  and  $I_2$  are linear polarised and have the same direction of polarisation vector. The laser beam  $I_1$  passes through the set of neutral filters (3) and illuminates the test-object (4). The signal from the object passes through the transparent glass plate (5), with a thickness of 20 mm, and with a help of an objective (6) focuses on the matrix of digital camera (7).

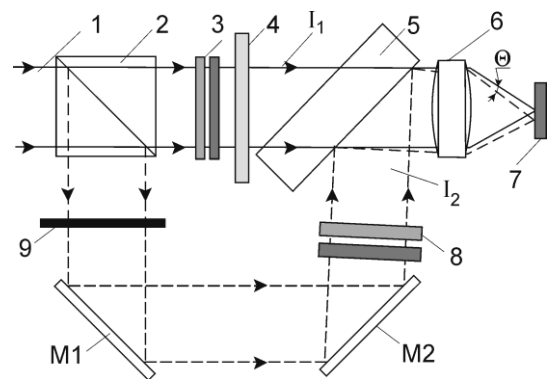


Fig. 1. Experimental setup: 1. Plane-parallel laser beam  $\lambda = 532 \text{ nm}$ , 2. Cube-divider, 3. Set of neutral filters, 4. Test-object, 5. Transparent glass plate, 6. Objective, 7. Digital camera matrix, 8. Set of neutral filters, 9. Shutter

The DCC1545M-GL ThorLabs monochromatic camera with parameters: resolution power  $1280 \times 1024 \text{ px}$ ; matrix size  $5.32 \text{ mm} \times 6.66 \text{ mm}$ ; and, pixel size  $5.2 \mu\text{m} \times$

5.2  $\mu\text{m}$ , is used for image recording. The transparent symbol  $F$  on the opaque background is used as the test-object. The second laser beam  $I_2$  (when the shutter 9 is open) is projected by mirrors  $M1$  and  $M2$  through the set of neutral filters (8) onto the surface of the glass plate (5). The reflected from the plate signal is projected by the objective (6) onto the digital camera matrix (7). The plate thickness of 20 mm is selected so that the signal  $I_2$  reflected from the back plane of the plate does not get to the matrix. The photo-detector S120VC - PM100 USB ThorLabs is used to measure the light signals. Instead of the digital camera, the photo-detector is placed in the same axial plane during the measurements. When the shutter is open (9, Fig. 1), the matrix of the digital camera is illuminated by the additional beam  $I_2$ , which does not illuminate the test-object. Using the mirrors  $M1$  and  $M2$ , the beam  $I_2$  is projected onto the matrix at an angle  $\Theta$  and an interference pattern is formed, the period of which depends on the wavelength of the laser radiation and the convergence angle  $\Theta$  on the beams  $I_1$  and  $I_2$ . Eq.1 shows the power density distribution in the formed interference pattern [5]:

$$I = I_1 + I_2 + 2\sqrt{I_1 I_2} \cos \varphi \quad (1)$$

where  $\varphi$  is the phase difference.

From formula Eq.1 it follows that the maximal and minimal power densities of the interference pattern are described by the Eq.2 and Eq.3 [5]:

$$I_{max} = I_1 + I_2 + 2\sqrt{I_1 I_2} \quad (2)$$

$$I_{min} = I_1 + I_2 - 2\sqrt{I_1 I_2} \quad (3)$$

As can be seen from Eq.3 at equal beam power densities  $I_1 = I_2$ , the minimal power density of the fringe pattern is  $I_{min} = 0$  and the maximal power density, according to Eq.2, is four times bigger than the power densities of the beams  $I_1$  and  $I_2$ . Eq.4 shows the Michelson fringe visibility (fringe contrast) of interference pattern [6]:

$$V = \frac{I_{max} - I_{min}}{I_{max} + I_{min}} \quad (4)$$

If the laser beams  $I_1$  and  $I_2$  are monochromatic with the same polarization, then the predicted Michelson visibility follows Eq.5 [7]:

$$V = \frac{2\sqrt{I_1 I_2}}{I_1 + I_2} \quad (5)$$

Let the minimal power density from the object that can be registered by digital camera (power density threshold  $I_{th}$ ) will be denoted as 1 conventional unit  $I_{th} = 1$ . If, using filters (3 and 8, Fig. 1), the power density of beams  $I_1$  and  $I_2$  is also set equal to  $I_1 = I_2 = I_{th} = 1$ , then, the visibility of interference fringes will be maximal  $V=1$  (Eq.5). However, the contrast of recorded image depends on the  $I_{th}$  of the digital camera used. Fig. 2a shows the

power density distribution of fringe pattern, formed by laser beams with equal power densities in the coordinate range  $X1$  and  $X2$ .

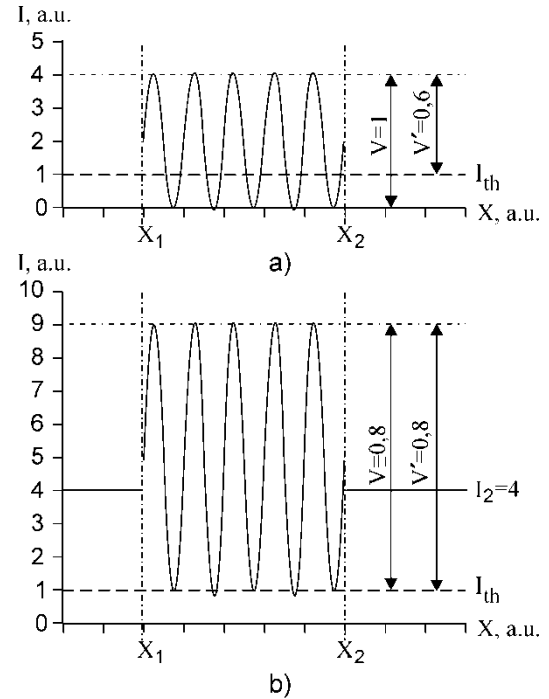


Fig. 2. Power density distribution of the fringe pattern

The fringe pattern visibility is  $V = 1$ , but the power density of the interference pattern in the range from 0 to 1 is less than the  $I_{th}$  of the digital camera (Fig. 2a). Denote the visibility of the recorded interference pattern as  $V'$ . The visibility of the recorded interference pattern is calculated from  $I_{min}=1$ ,  $I_{max}=4$  and, according to Eq.4,  $V' = 0.6$ . To register an image with a higher fringe contrast, it is necessary to set such beam power density  $I_2$ , that the minimal power density of the interference lines will be equal to the power density threshold  $I_{min}=I_{th}$ :

$$I_{min} = I_1 + I_2 - 2\sqrt{I_1 I_2} = I_{th} \quad (6)$$

Express  $I_2$  in terms of  $I_1$  and  $I_{th}$  from equation (6). The equation (6) has two solutions:

$$I_2 = I_1 + I_{th} + 2\sqrt{I_1 I_{th}} \quad (7a)$$

$$I_2 = I_1 + I_{th} - 2\sqrt{I_1 I_{th}} \quad (7b)$$

The parameter  $I_2$  can be negative in equation (7b), but this has no real physical meaning in this experiment. The solution (7a) will be used to calculate the power density  $I_2$ . In this case for  $I_1 = I_{th} = 1$  the beam power density  $I_2=4$  (Eq.7a),  $I_{max} = 9$  (Eq.2), and  $I_{min}=1$  (Eq.3). The visibility of the recorded fringe pattern will be  $V' = 0.8$  (Fig. 4b).

Further, for each value of the beam power density from the object  $I_1$ , which is less than the power density

threshold, the beam power density  $I_2$  can be calculated from the Eq.7a.

### 3. Results and discussion

Images were recorded at the shortest possible exposure time (0.04 ms) of the digital camera used. Fig. 3a shows the image of the symbol  $F$  recorded by a digital camera in the absence of the second laser beam  $I_2$  (shutter 9, Fig. 1 is closed). The power density of the beam from the object  $I_1$  was selected so that the recorded image had the maximal contrast.

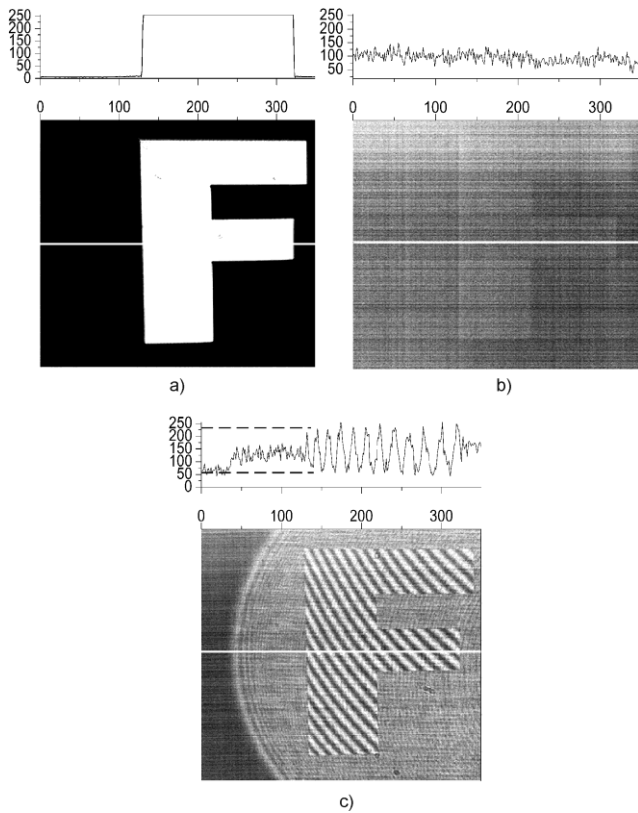


Fig. 3. The recorded images of the symbol  $F$ : a) maximal contrast; b) object beam power density  $I_1=477\text{nW/cm}^2$ ; c) object beam power density  $I_1=477\text{nW/cm}^2$  and  $I_2=1.93\ \mu\text{W/cm}^2$

The image was processed by a graphical editor to allow determining pixel-by-pixel distribution of the grey scale along to the frame [8-9]. Through the image centre a 1-px-thick line (white line, Fig. 3a) was picked out and the pixels brightness distribution (from 0 to 255 of the grey scale) was obtained (the top of Fig. 3a). As can be seen from Fig. 3a, the image of the symbol  $F$  is recorded with maximal contrast.

To determine the power density threshold  $I_{th}$ , the power density from the object  $I_1$  was reduced to the minimal value, at which the image of the symbol  $F$  can still be distinguished. The software of the digital camera

allows observing the image in real time on the computer screen, and using the auto-scale option to select the optimal value of image brightness from 0 to 255 of the grey scale. Fig. 3b shows the image of the symbol  $F$ , which was recorded at the beam power density of  $I_1=477\text{nW/cm}^2$  and grey scale in the range from 3 to 9 (auto-scale option of digital camera software). Image processing in the graphics editor showed a high level of noise, but the image of the symbol  $F$  can still be visually recognized. Assume that  $I_{th} = 477\ \text{nW/cm}^2$  is the power density threshold for digital camera used. The same image was recorded using the beam power density  $I_2=1.93\ \mu\text{W/cm}^2$ , the power density of which was calculated by Eq.7a. Fig. 3c shows the image of the symbol  $F$  recorded at the beam power density from the object  $I_1=I_{th}=477\text{nW/cm}^2$  and  $I_2=1.93\ \mu\text{W/cm}^2$ . As can be seen from the power density distribution diagram (the top of the Fig. 3c), the image can be recognized as the contrast of the dark and light lines of the fringe pattern. The period of the interference pattern is  $d\sim 0.14\ \text{mm}$  and the slope of the interference lines is  $\sim 45^\circ$ . The polarization vector of the laser radiation is directed parallel to the interference lines. The average visibility of recorded fringe pattern (dashed lines, Fig. 3c) is  $V\sim 0.63$ , although at  $I_1=477\text{nW/cm}^2$  and  $I_2=1.93\ \mu\text{W/cm}^2$  the visibility of the fringes (according to Eq.5) should be  $V=0.8$ . The reduced visibility  $V'$  can be explained by several factors: the noise of a digital camera with a gray scale in the range from 3 to 9; phase changes of the laser beams  $I_1$  and  $I_2$  when they pass through the optical filters (3 and 8, Fig. 1); and, the objective (6, Fig. 1). Also, plane-parallel laser beams  $I_1$  and  $I_2$  become spherical after passing through the objective. As a result, the interference pattern is formed as the interference of two spherical beams, which is observed in the image in the form of curved interference lines. However, as can be seen from Fig. 3c, the image of the object  $F$  is quite well recognizable, comparative to the image in Fig. 3b, despite the fact that both images were recorded at the same power density from the object  $I_1=I_{th}=477\text{nW/cm}^2$ . At the power density from the object  $I_1=392\text{nW/cm}^2$ , the symbol  $F$  is not observed in the recorded image, and longitudinal scanning in graphical editor shows inhomogeneous noise at the level of 50 - 100 of grey scale (Fig. 4a). Fig. 4b shows the image of the symbol  $F$  recorded at the beam power density from the object  $I_1=392\text{nW/cm}^2$  and a beam power density  $I_2=1.75\ \mu\text{W/cm}^2$ . As can be seen from Fig. 4b, the image of the object  $F$  is well recognizable. The averaged visibility of recorded interference fringes is  $V'\sim 0.57$ . Decreasing of the beam power density from the object to  $I_1=135\ \text{nW/cm}^2$ , which is 3.5 times less than  $I_{th}$ , requires the increase of the beam power density  $I_2$  (conform Eq. 7a) to  $I_2=1.13\ \mu\text{W/cm}^2$ .

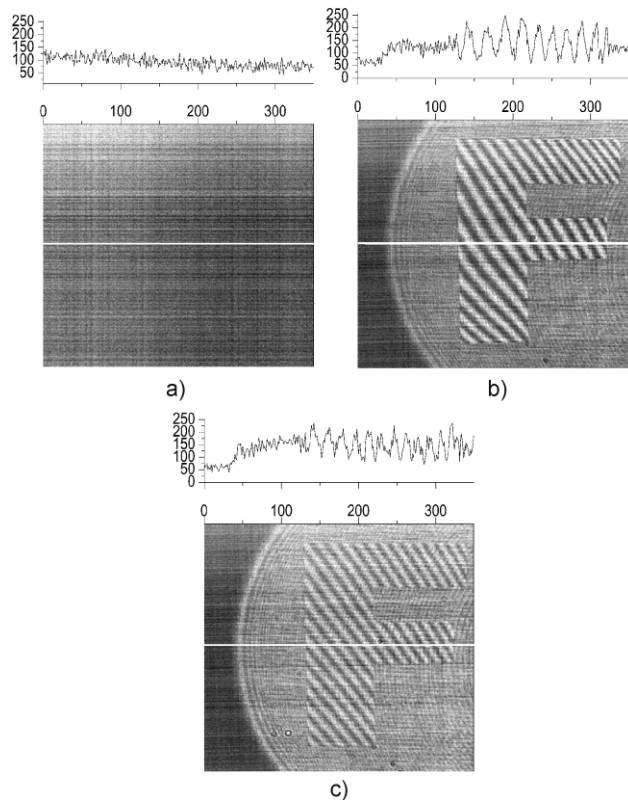


Fig. 4. The recorded image of the symbol  $F$ : a) object beam power density  $I_1=392 \text{ nW/cm}^2$ , b) object beam power density  $I_1=392 \text{ nW/cm}^2$  and  $I_2=1.75 \text{ } \mu\text{W/cm}^2$ , c) object beam power density  $I_1=135 \text{ nW/cm}^2$  and  $I_2=1,13 \text{ } \mu\text{W/cm}^2$

Fig. 4c shows the image of the symbol  $F$  recorded at the power densities  $I_1=135 \text{ nW/cm}^2$  and  $I_2=1.13 \text{ } \mu\text{W/cm}^2$ . The average visibility of recorded interference fringes is  $V' \sim 0.34$ .

Studies were conducted on the registration of images while the power density from the object to the limit value  $I_l$ , at which it is still possible to recognize image of the symbol  $F$ . Fig. 5a shows the image of the symbol  $F$  recorded at the power densities  $I_1=52 \text{ nW/cm}^2$  and  $I_2=849 \text{ nW/cm}^2$ .

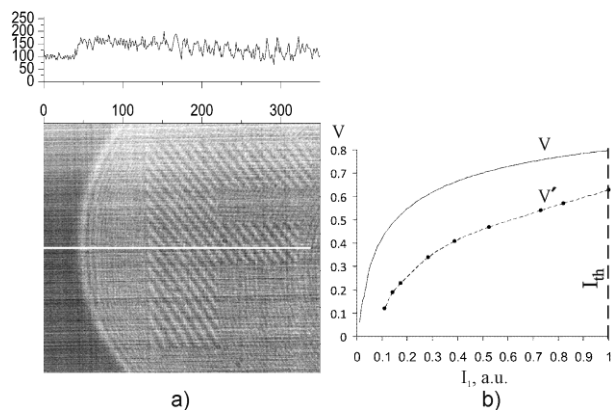


Fig. 5. a) The recorded image of the symbol  $F$ : object beam power density  $I_1=52 \text{ nW/cm}^2$  and  $I_2=849 \text{ nW/cm}^2$ , b) The theoretical fringe pattern visibility  $V$  and obtained experimentally  $V'$

The average visibility of recorded fringe pattern is  $V' \sim 0.12$ . The recorded image of the symbol  $F$  can still be recognized, despite the fact that the power density from the object  $I_l$  is almost nine times less than the power density threshold  $I_{th}$  for digital camera used.

To compare the theoretical and experimental results, the power density threshold  $477 \text{ nW/cm}^2$  is equated to one conventional unit. Fig. 5b shows the dependence of the visibility of fringe pattern  $V$ , calculated by Eq. 5, and the obtained experimental results  $V'$  depending on the power density from the object  $I_l$ , which is less than the  $I_{th}$ . The experimental results differ from the theoretical results that were discussed above. However, the studied object can be recognized when the power densities from the object are lower than the  $I_{th}$ . It should be noted that in the optical scheme a simple glass plate is used (5, Fig. 1) with a thickness of 20 mm, the transmittance of which is only 86% (for the wavelength 532 nm). The beam from the object is attenuated due to the reflection of the signal from both surfaces of the plate. In practice, the double-sided anti-reflective coating plate can be used, which allows reducing the reflectance to the minimum.

#### 4. Conclusion

The study of photosensitive objects, or objects weakly sensitive to light, may require the decrease of the power density from the object less than the power density threshold for digital camera. Illumination of the object under study by a coherent radiation source can make it possible to register an image of the object at power densities lower (no less than nine times) than the power density threshold for digital camera used.

#### Acknowledgments

This research was supported by institutional project # 20.80009.5007.12 carried out at Moldova State University.

#### References

- [1] A. White, J. Mitchell, O. Nairz, P. Kwiat, Phys Rev A. **58**(1), 605 (1998).
- [2] Y. J. Jung, Opt. Express **25**(10), 12029 (2017).
- [3] G. Li, L. Zhao, M. Zhou, M. Wang, L. Lin. Appl Optics. **52**(33), 7934 (2013).
- [4] A. Chirita, T. Galstian, M. Caraman, V. Prilepov, O. Korshak, I. Andries, Optoelectron. Adv. Mat. **7**(3-4), 293 (2013).
- [5] M. Born, E. Wolf, "Principles of Optics", 7th ed. Cambridge University Press, Cambridge, p. 259 (1999).
- [6] R. Collier, K. Burckhardt, L. Lin. "Optical Holography", Academic, New York, p. 26, (1971).
- [7] T. Qureshi. Quanta **8**(1), 24 (2019).
- [8] A. Chirita, F. Dimov, N. Kukhtarev, J. Nonlinear Opt. Phys. **26**(4), 1750046 (2017).
- [9] A. Chirita, N. Kukhtarev, O. Korshak, V. Prilepov, Iu. Jidcov, Laser Phys. **23**(3), 909 (2013).

\*Corresponding author: arc\_chirita@yahoo.com